# Model–based Registration of X–ray Mammograms and MR Images of the Female Breast

N. V. Ruiter, R. Stotzka, *Member, IEEE*, T. O. Müller and H. Gemmeke, *Member, IEEE*

***Abstract*— We present a new approach for automatic registration of X–ray mammograms and MR images. Multimodal breast cancer diagnosis is supported by automatic localization of small lesions, which are only visible in the mammograms or the MR image. To cope with the huge deformation of the breast during mammography, a finite element model of the deformable behavior of the breast is applied during the registration.**

**An evaluation of the registration with six clinical data sets resulted in an accurate localization with a mean displacement of 4.3 mm (± 1 mm) and 3.9 mm (± 1.7 mm) for predicting the lesion position in mammograms and in the MR images, respectively.**

***Index Terms*— Registration, multimodal, finite element simulation, deformation model of the breast.**

## I. Introduction

X–RAY mammography is the standard method for image–guided breast cancer diagnosis, yet (X-ray) mammograms are 2D projections of a deformed breast. For further treatment or for combination with other imaging methods, e.g. Magnetic Resonance (MR) Imaging, the relationship between the undeformed and the deformed breast has to be determined. The main objective of this work was to develop a method for the automatic localization of the 3D position of a lesion in a MR image based on the position of that lesion in two standard mammograms and vice versa. The displacement of the position estimate has ideally to be within 5 mm to be applicable for early breast cancer diagnosis.

The central problem in registration of mammograms and MR images is the large deformation of the breast during mammography. The breast has to be squeezed between two plates and is compressed up to 50% in diameter to obtain mammograms with good image contrast. This complex 3D deformation of the breast is only recorded as a 2D projection, thus the individual 3D configuration of the deformed breast cannot be reconstructed. Additionally, the deformation of the breast depends on the positioning and the shape of the breast and its composition varies extremely between patients. Therefore the exact projection angle, the amount of imaged tissue, the applied compression force and the thickness of the compressed breast are unknown for the individual case. Note: The medical term ”breast compression” will be used throughout this paper as it is commonly used for the applied breast deformation during mammography. In a physical sense the breast tissue, consisting mainly of water, is incompressible.

Manuscript received October 16, 2004.

All authors are with Forschungszentrum Karlsruhe, Institute of Data Processing and Electronics, Postfach 3640, 76021 Karlsruhe, Germany. (email: {ruiter,stotzka,mueller,gemmeke}@ipe.fzk.de)

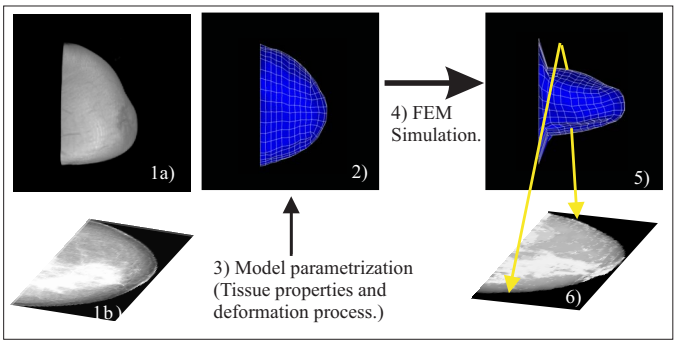


Fig. 1. Registration strategy: 1a) MR image and 1b) mammogram. 2) Patient specific finite element mesh. 3) Formulation of the tissue properties and the deformation process. 4) Simulation. 5) Deformed finite element model. 6) Projection of a generated MR image of the deformed breast.

Only three approaches for registering mammograms and MR images have been proposed until now. In a first approach our group [1] used a non–linear scaling algorithm to calculate the specific projection angle of an individual projection and to register mammograms to MR images. The mean displacement of the registration of the six clinical data sets as used in this paper was approx. 8 mm. Behrenbruch et al [2] used the breast boundary and internal landmarks to register mammograms to so–called pharmacokinetic projections of the corresponding MR images. Their approach showed an average error of 4 to 5 mm in overlap of the multimodal lesions in seven cases. They only applied the registration to data sets where the lesion is visible in both modalities and included the lesion as salient structure in the landmark detection process. Marti et al [3] also used internal landmarks to register mammograms to MR projections. They evaluated the plausibility of the found projection angle with one case. All approaches registered mammograms with direct projections of the undeformed breast in the MR image. Therefore the 3D effects of the deformation are not included.

In this paper a novel method for automatic registration of mammograms and MR images of the female breast is proposed. The registration includes a biomechanical model of the deformable behavior of the breast to overcome the problems associated with the huge deformation during mammography. The model allows to deform the undeformed breast in 3D, as given in the MR image, to adopt the same configuration as in

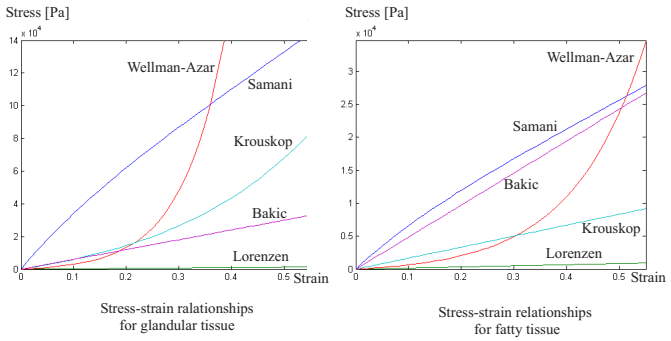


Fig. 2. Overview of the applied material models as stress–strain relationships for glandular tissue (left image) and fatty tissue (right image) in the strain range between 0% and 55%. Stress is given in $[Pa]$. Note the different maximum stresses for glandular and fatty tissue.

a corresponding mammogram. Thus a subsequent projection of the deformed MR image includes the 3D effects of deformation and can be compared directly to the mammogram. A summary of this registration strategy is given in Fig. 1.

## II. Construction of the Biomechanical Model

For appropriate modeling of the deformable behavior of the breast, a simulation model based on the finite element method (FEM) capable of large deformations and non–linear (nearly) incompressible materials [4] was built. The simulations were calculated using the commercial tool ANSYS [5].

The model is comprised of parameters for the applied meshing method, the used number and type of finite elements, the underlying material models of the breast tissues, and the assigned boundary conditions, i.e. the formulation of the deformation process. The applied methods are presented and discussed in the following subsections.

### A. Automatic Mesh Generation

The meshing, i.e. the discretization of the object, is accomplished automatically based on a segmented MR image. The MR image is divided into skin, fatty and glandular tissue. The transfinite interpolation method [6] for meshing is applied. In general the soft breast tissue is supposed to be incompressible [7], therefore the recommended hexahedral finite elements capable of nearly incompressible behavior are employed [8]. The number of finite elements used for simulation was $7^3$, which was found experimentally as trade–off between accuracy and calculation time.

### B. Plausible Material Models for Breast Tissues

Different material models for fatty and glandular breast tissue as proposed in literature have been examined in respect to the plausibility of the resulting deformation force and the accuracy of the simulation. The following models have been considered: Wellmann [9], Azar [7] and Krouskop et al [10] proposed exponential, Samani et al [11] neo-hookean hyperelastic and Bakic [12] and Lorenzen et al [13] linear elastic stress–strain relationships. The models differ not only in the mathematical formulation of the stress–strain relationship but also in the actual material parameters, i.e. the hardness of the tissues. An overview of the different models for glandular and fatty tissues is displayed in Fig. 2. Note: The model of Azar follows the material model of Wellman closely. He introduced an hardening of fatty tissue to simulate the effects of the Cooper's ligaments. This is included in the simulations, but not depicted in the figure.

A fundamental requirement for a material model is its plausibility in terms of the compression force necessary to deform the breast. Sullivan et al [14] measured the applied forces during mammography for 560 patients in the range of 49 to 186 N, the median was found to amount to 127 N. He also measured the diameter of the breasts during compression, but did not give a correlation between the thickness change and the compression force. Therefore only the principal limits of the compression force could be evaluated, the extent of the deformation for lower (21%) and higher (50%) mammographic compression were estimated based on clinical data. In a simple experiment a middle sized breast was approximated by a cube of the volume 240 $cm^3$. For the approximation of the lower force limit, the forces were calculated for 21% compression of the cube consisting of the softer fatty tissue. The upper limit on the compression force was approximated for a 50% compression of the cube consisting of the harder glandular tissue. The results are displayed in Table I. The limits on the compression force for the different material models were in most cases not realistic. Only the material models of Krouskop and Bakic resulted in a realistic range.

To obtain the plausibility of the simulated deformation a specially acquired data set was used, consisting of two MR images of a healthy volunteer, one displaying an undeformed breast, the other showing the same breast, subjected to mammographic

TABLE I

Applied compression force as result of the different material models.

| | Wellman / Azar | Samani | Krouskop | Bakic | Lorenzen |
|---|---|---|---|---|---|
| 21% (fat) | 9 | 58 | 14 | 39 | 1 |
| 50% (gland) | 2217 | 513 | 262 | 116 | 5 |

The forces for an overall compression of 21% assuming only fatty tissue, and 50% assuming only glandular tissue are displayed in $[N]$, rounded. Sullivan's measured values ranged between 49 N and 186 N, with a median of 127 N.

TABLE II

Distances of landmarks with different material models.

| | Wellm. | Azar | Samani | H. tiss. | Krouskop | Bakic | Loren. |
|---|---|---|---|---|---|---|---|
| $\mu$ | 3.1 | 3.1 | 3.1 | 3.1 | 3.1 | 3.3 | 3.4 |
| SD | 1.4 | 1.3 | 1.4 | 1.3 | 1.3 | 1.5 | 1.4 |
| max | 5.1 | 5.0 | 4.8 | 5.0 | 5.1 | 5.8 | 5.7 |

Mean landmark distance ($\mu$), standard deviation (SD) and maximum distance (max) of simulations using different material models. In $[mm]$, rounded. The mean distance of the landmarks before simulation was 18 mm, the maximum distance 26 mm. (Wellm. is short for Wellman, H. tiss. for homogenous tissue and Loren. for Lorenzen)

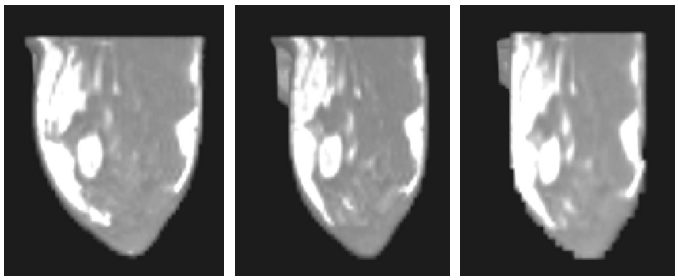

Fig. 3. Qualitative comparison of the simulated MR image to the real MR images. Left: Cut through undeformed breast. Middle: Cut through deformed breast. Right: Cut through breast in artificially generated MR image after simulation.

compression with 21% decrease in diameter. The simulation of the deformation was carried out using the undeformed MR image to build the finite element model. Additionally to the models of the literature we used a neo–hookean material model assuming only one tissue type in the breast, the "homogenous tissue model". The results of the deformation were compared to the real deformed breast by 17 landmarks. The deviation of the landmarks is given in Table II and an example of the correspondence between the simulated and the real deformed MR image in Fig. 3. All material models gave similar results. Therefore the simple homogenous tissue model was chosen for further experiments, approximating the material model for glandular tissue as given by Bakic to obtain realistic compression forces.

When the landmark displacements were viewed for different coordinate directions, the error was found to be most pronounced in the lateral elongation of the breast. It was significantly smaller than the real elongation. We call this problem "macroscopic anisotropy" in the remainder of this paper. One reason for this macroscopic anisotropy is certainly that modeling only fatty and glandular tissue is a very simplified description of the breast's internal structures. The breast consists of ducts, lobes, connective tissue, fat, lymphatics, blood vessels and nerves, with E–moduli for the individual tissue types ranging from 1 up to 1000 kPa. The tissue structures depict a pronounced structuring of the breast, e.g. the connective tissue embeds the fatty tissue parts of the breast in the honeycomb structures of the Cooper's ligaments [7]. This could limit the inherently isotropic structures in certain directions and therefore add to anisotropic behavior. All this structures are too small to be visible in the MR images and thus cannot be modeled in this approach. Additionally, the effects of the enclosing skin were neglected so far. To cope with this problem two different approaches will be examined in the Subsections II-C and II-D.

### C. Boundary Conditions

Any deformation process in FEM is formulated by application of loads at certain nodes. Since the force applied in mammography is usually not recorded, displacements are applied as predefined loads in this approach.

The mammographic compression is mimicked in an first approach by adding compression plates into the simulation model ("plate compression"). The deformation is formulated by moving the compression plates until a certain amount of compression is achieved, and is solved as contact problem. The individually varying thickness of the breast after deformation is approximated using the diameters of the breast in the MR image and in the mammogram. The thickness of the compressed breast is then applied as stop criterion for the deformation.

In a second approach ("updated boundary conditions") the information of the projected image of the deformed breast is added to the results of the plate compression in a two–step simulation: In the first step plate compression is applied. In the second step the shape of the now deformed breast and the circumference of the corresponding mammogram are used to estimate the 3D shape of the breast. The boundary conditions for this simulation are then formulated as displacements between the undeformed and deformed surface of the estimated 3D shape. This results in a MR projection of the deformed breast with exactly the same circumference as in the mammogram.

TABLE III

DISTANCES OF LANDMARKS WITH DIFFERENT BOUNDARY CONDITIONS.

| | Plate compression | Additional points | Updated boundary cond. |
|---|---|---|---|
| $\mu$ | 3.1 | 2.6 | 2.7 |
| SD | 1.3 | 1.3 | 1.1 |
| max | 5.0 | 4.6 | 4.3 |

Average landmark distance ($\mu$), standard deviation (SD) and maximum distance (max) of simulations with different boundary conditions. In $[mm]$, rounded. (Updated boundary cond. is short for updated boundary conditions.)

The results of a landmark comparison for the volunteer data set with different boundary conditions are given in Table III. Simulations using only plate compression gave a mean displacement error of 3.1 mm (standard deviation $\pm$ 1.3 mm). However, the maximal displacement was at the accuracy limit of 5 mm due to the macroscopic anisotropy. Simulations using additional information of the deformed location of 16 surface points, had an overall accuracy of 2.6 mm ($\pm$ 1.1 mm). The maximal error was well below the limit of 5 mm. The method of updated boundary conditions gave similar good results, decreasing the maximum displacement even further.

### D. Modeling of Skin

No literature describing the connection between the skin and the breast interior quantitatively was available, therefore four models were designed to test possible manifestations. The model without skin ("no skin") as used until now was compared to tightly attached skin ("attached"), and skin modeled as enclosing membrane with different friction, i.e. perfect sliding ("sliding") and perfect adherence ("adherent").

The linear elastic material model proposed by Samani et al [11] is applied for skin. They assume for strains below 50% a constant E–modulus of 10 kPa. The results are displayed as mean and maximum landmark distances in Table IV. Additionally to the Euclidian distances, distances in the critical lateral direction are given.

TABLE IV

RESULTS OF SIMULATIONS WITH DIFFERENT SKIN MODELS.

| | No skin | Attached | Sliding | Adherent |
|---|---|---|---|---|
| Euclidian distances | 3.4 (5.4) | 3.3 (4.5) | 3.9 (5.3) | 3.9 (5.4) |
| Lateral distances | 2.6 (4.7) | 2.1 (3.5) | 1.8 (3.3) | 1.8 (3.7) |

Mean and maximum (in brackets) Euclidian distance and lateral distance in [mm], rounded.

It could be confirmed that the modeling of skin improves the lateral accuracy of the simulation, as all simulations including skin gave better results as well in mean as in maximum distance in this direction. But the distances in all other directions were increased, resulting in a smaller overall accuracy for the membrane models. Only the attached skin model improved the simulations. In comparison to the results of the simulations with updated boundary conditions a similar maximum distance could be achieved, but the mean landmark distance was significantly larger for the attached skin model. The results indicate that the macroscopic anisotropy of the simulation model can be partly explained by the influence of skin on the deformation. Since modeling of skin would increase the complexity of the FEM model considerably, for the purposes of this application the updated boundary condition approach is favored.

## III. REGISTRATION USING THE DEVELOPED MODEL

Registration provides the direct comparability of the matched images. In our simulation approach this is ensured by an appropriate formulation of the deformation process, so that the deformed breast in the simulation is similar (ideally equal) to the compressed breast, as imaged in the corresponding mammogram.

First the exact projection angle and the imaged portion of the breast of the mammogram are calculated, using our earlier registration approach [1]. After that the simulation model is built, using the MR image and physical properties of the breast tissues by the homogenous tissue model. The updated boundary approach showed the best accuracy in deforming the breast while building the deformation model and is therefore used for the registration.

To locate the position of a lesion in the mammogram, its known position in the MR image is projected from the deformed MR image, this projected position can then be transferred directly to the registered mammogram. To recover the volume in the MR image containing a lesion known in the two standard mammograms, the registration approach described above has to be accomplished for both mammograms. After the registration, the position of the lesion in the mammogram can be superimposed directly onto the particular MR projection. Knowing the deformation applied to the undeformed breast, the actual position of the lesion in can be calculated by applying the inverse transformation.

## IV. LOCALIZATION ACCURACY WITH CLINICAL DATA SETS

The localization accuracy of the registration approach was evaluated using six clinical data sets. The lesion position was known in both mammograms and the corresponding MR image, so that the simulated location and the real location could be compared. The distance of the center of the lesion and the overlapping area or volume are given in Table V and VI. The lesion in data set 2 was not visible in the oblique mammogram, therefore it could not be used in the evaluation of the localization accuracy in the mammogram. The localization of the lesion position in the MR image of data set 2 is an estimate based on the cranio–caudal mammogram.

TABLE V

RESULTS OF LESION LOCALIZATION IN THE MAMMOGRAMS.

| Data set | Rigid regist. | Plate compression | Updated boundary |
|---|---|---|---|
| Data set 1 cc. | 20.3 (0%) | 20.4 (0%) | 3.7 (40.7%) |
| Data set 2 cc. | 25.4 (0%) | 22.9 (0%) | 4.3 (85.7%) |
| Data set 3 cc. | 29.0 (0%) | 6.0 (80%) | 5.0 (100%) |
| Data set 4 cc. | 24.0 (0%) | 12.2 (10.9%) | 2.3 (100%) |
| Data set 5 cc. | 6.7 (27.7%) | 31.0 (0%) | 4.0 (86.7%) |
| Data set 6 cc. | 36.3 (0%) | 20.3 (0%) | 4.2 (84.6%) |
| Data set 1 obl. | 28.1 (0%) | 25.7 (0%) | 6.0 (35.5%) |
| Data set 3 obl. | 32.3 (0%) | 22.3 (0%) | 4.4 (83.4%) |
| Data set 4 obl. | 14.0 (0%) | 10.8 (10.7%) | 4.0 (78%) |
| Data set 5 obl. | 23.9 (0%) | 31.0 (0%) | 3.4 (100%) |
| Data set 6 obl. | 19.7 (0%) | 14.4 (25%) | 6.0 (100%) |

The center lesion displacement and percentage of lesion area overlap (in brackets) are given for rigid, plate compression and updated boundary conditions registration (in mm and percent, rounded). The first six rows describe experiments using the cranio–caudal mammograms, second five rows describe experiments using the oblique mammograms. Rigid regist. is short for rigid registration.

TABLE VI

RESULTS OF LESION LOCALIZATION IN THE MR IMAGES.

| Data set | Rigid registration | Plate compression | Updated boundary |
|---|---|---|---|
| Data set 1 | 86.5 (0%) | 17.4 (2.2%) | 4.6 (88.9%) |
| Data set 2 | (25.4 (0%)) | (22.9 (0%)) | (3.2 (99.6%)) |
| Data set 3 | 109.5 (0%) | 12.2 (44.0%) | 5.4 (58.9%) |
| Data set 4 | 65.1 (0%) | 6.2 (100%) | 1.6 (100%) |
| Data set 5 | 81.0 (0%) | 19.4 (15.9%) | 6.2 (100%) |
| Data set 6 | 118.3 (0%) | 9.2 (82.4%) | 2.2 (100%) |

The distance of center points and the percentage of lesion volume overlap (in brackets) in 3D (In mm and percent, rounded.) are given. For description of column names see table V.

A simple rigid alignment is, as expected, not capable of mammogram and MR image registration. Registration using plate compression improves the alignment of the images, but does not meet the accuracy requirements. The effect of macroscopic anisotropy during plate compression could also be observed with the clinical data.

Updated boundary conditions based registration predicts for all cases the center of the lesion within the original lesion area or volume. The mean displacement of the center of a lesion of 4.3 mm (standard deviation $\pm$ 1 mm) for predicting the lesion position in mammograms, and a mean center distance of 3.9 mm ($\pm$ 1.7 mm) estimating the lesion position in the MR images were found. This equals an improvement of 78% and 94% compared to a simple rigid registration. In more than three quarters of the lesion position estimates the center distances were well below the accuracy limit of 5 mm, and the maximum value was not more than 6.2 mm. Additionally, mimicking the X–ray imaging process in projections of the deformed MR

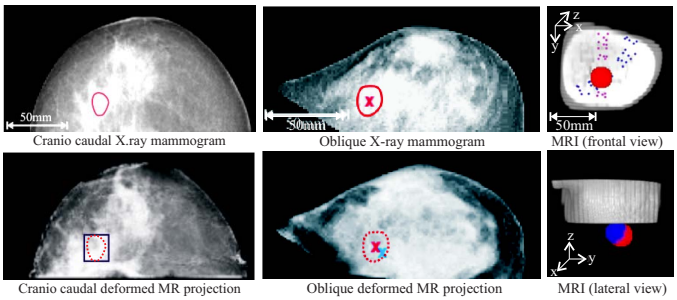


Fig. 4. Exemplary localization results. First two columns show mammograms and the corresponding MR projections with lesion localization. The third column depicts the lesion localization in a MR image. The original lesions are depicted in red, the localization in blue.

images resulted in images very similar to the mammograms. Exemplary results are displayed in Fig. 4.

## V. Discussion and Conclusion

We developed a new model–based method to register mammograms and MR images of the breast, which overcomes the problems due to the large deformation of the breast during mammography. This approach determines the relationship between the mammographically deformed breast and the undeformed breast automatically.

We demonstrated, that a material model with the same physical tissue properties for all breast tissues is sufficient, and more complex models do not increase the simulation accuracy. This simple homogenous tissue model approximates a linear elastic model by a neo–hookean model to achieve better solvability in case of nearly incompressible materials [8]. In a homogenous body with linear elastic material the simulated displacements are not sensitive to changes of the size of the stiffness parameter of the material model. For a realistic compression force the material model only has to be scaled with an adequate stiffness parameter, for example a neo–hookean approximation of the Bakic model.

Experiments considering different boundary conditions have been presented. Using a 3D data set of a compressed breast, we showed that mimicking plate compression is not sufficient for the required simulation accuracy, as the breast shows anisotropic behavior. Therefore a method was developed to estimate the 3D shape of the deformed breast based on the result of a first plate compression simulation and the circumference of the breast as given in the corresponding mammogram. With this updated boundary conditions approach, it was possible to simulate the deformation with a maximum displacement of 4.3 mm, well below the required accuracy limit.

In a strict sense the evidence of the deformation model of the breast obtained with the volunteer MR images is limited to that data set. Additionally, the applied compression of this data set of an overall strain of 21% is in the lower range of the compression applied during mammography. In spite of that a first evaluation with six clinical data sets showed that the deformation model is sufficient to locate even the smallest lesions. In all cases the estimated center of the lesion lay within the actual lesion area or volume and is therefore adequate for biopsy. The next step is therefore to evaluate the registration in a clinical study with a larger set of data.

The simulation model is based on conventional MR data sets with a voxel size of $(1.4\,\mathrm{mm})^3$, excluding smaller tissue structures, e.g. Cooper's ligaments, from the model. For future work it will be interesting to build a more complex breast model based on 3D data of higher spatial resolution. For the same patients mammograms with known compression and applied force will be needed. Then a more detailed model including different tissue models could be built.

Additional applications of this approach are the support of biopsy or surgical interventions, e.g. MR image guided biopsy of lesions only visible in mammograms.

## References

[1] T. O. Müller, N. V. Ruiter, R. Stotzka and W. A. Kaiser, "Automatic matching of MR volume data and X–ray mammograms", *Europ. Radiol.*, vol. 10, no. 9, 2000.

[2] C. P. Behrenbruch, M. Yam, M. Brady and R. E. English, "The use of Magnetic Resonance imaging to model breast compression in X–ray mammography for MR/X–ray data fusion", $5^{th}$ *Proc. Int. Works. Digital Mammography*, Toronto, Canada, 2000.

[3] R. Marti, C. Rubin, E. Denton and R. Zwiggelaar, "Mammographic X–ray and MR correspondence", $6^{th}$ *Proc. Int. Works. Digital Mammography*, Bremen, Germany, 2002.

[4] O. C. Zienkiewicz and R. L. Taylor, *The finite elemente method – volume 2*, Butterworth Heinemann, $5^{th}$ edit., 2000.

[5] ANSYS, INC. www.ansys.com, Version 5.6.

[6] P. Knupp and S. Steinberg, *Fundamentals of grid generation*, CRC Press, 1993.

[7] F. S. Azar, *A deformable finite element model of the breast for predicting mechanical deformations under external perturbations*, PhD thesis, Univ. of Pennsyl., USA, 2001.

[8] P. Kohnke, *Ansys theory reference 5.6.*, 1999.

[9] P. S. Wellman, *Tactile imaging*, PhD thesis, Havard Univ., USA, 1999.

[10] T. A. Krouskop, T. M. Wheeler, F. Kallel, B. S. Garra and T. Hall, "Elastic moduli of breast and prostate tissues under compression", *Ultras. Imag.*, vol. 20, 1998.

[11] A. Samani, J. Bishop, E. Ramsay, and D. B. Plewes, "Large breast tissue deformation finite element modeling for MR/X–ray mammography data fusion", $5^{th}$ *Proc. Int. Works. Digital Mammography*, Toronto, Canada, 2000.

[12] P. R. Bakic, *Breast tissue description and modeling in mammography*, PhD thesis, Lehigh Univ., USA, 2000.

[13] J. Lorenzen, R. Sinkus, M. Lorenzen, M. Lorenzen, M. Dargatz, C. Leussler, P. Roschmann and G. Adam, "MR elastography of the breast: preliminary clinical results", *RoFo Fortschritte auf dem Gebiet der Röntgenstrahlen und der Bildgebenden Verfahren*, vol. 174, no. 7, 2002.

[14] D. C. Sullivan, C. A. Bean, S. M. Goodman and D. L. Watt, "Measurement of force applied during mammography", *Radiol.*, vol. 181, 1991.